

Transport on flexible Rydberg aggregates using circular states

M. M. Aliyu,¹ A. Ulugöl,¹ G. Abumwis,^{1,2} and S. Wüster^{1,3}

¹*Department of Physics, Bilkent University, Ankara 06800, Turkey*

²*Max Planck Institute for the Physics of Complex Systems,
Nöthnitzer Strasse 38, 01187 Dresden, Germany*

³*Department of Physics, Indian Institute of Science Education and Research, Bhopal, Madhya Pradesh 462 023, India**

Assemblies of interacting Rydberg atoms show promise for the quantum simulation of transport phenomena, quantum chemistry and condensed matter systems. Such schemes are typically limited by the finite lifetime of Rydberg states. Circular Rydberg states have the longest lifetimes among Rydberg states but lack the energetic isolation in the spectrum characteristic of low angular momentum states. The latter is required to obtain simple transport models with few electronic states per atom. Simple models can however even be realized with circular states, by exploiting dipole-dipole selection rules or external fields. We show here that this approach can be particularly fruitful for scenarios where quantum transport is coupled to atomic motion, in adiabatic excitation transport or quantum simulations of electron-phonon coupling in light harvesting. Additionally, we explore practical limitations of flexible Rydberg aggregates with circular states and to which extent interactions among circular Rydberg atoms can be described using classical models.

PACS numbers:

I. INTRODUCTION

We refer to flexible Rydberg aggregates as assemblies of Rydberg atoms that exhibit excitation transport or collective exciton states and are mobile in a possibly restricted geometry [1]. They exhibit links between motion, excitation transport and coherence [2–5] and spatially inflated Born-Oppenheimer surfaces for the simulation of characteristic phenomena from the nuclear dynamics of complex molecules [6–10].

Most related experiments [11–16] and theory in this direction have so far focussed on aggregates based on Rydberg states with low angular momentum, $l = 0, 1, 2$, due to the possibility of direct excitation and the energetic isolation provided by the energy gap to the next higher angular momentum states. For example $E(|n = 50, d\rangle) - E(|n = 50, p\rangle) = 151.7$ GHz in ⁸⁷Rb, which can be much larger than energy scales accessible by Rydberg aggregate dynamics. Here n is the principal quantum number. However inertia and spontaneous decay limit realistic flexible Rydberg aggregate sizes to less than $\sim 4 - 10$ atoms for these low angular momentum states.

Rydberg atomic properties are qualitatively changed in circular states, where angular momentum is maximised to $l = n - 1$ and pointing along the quantisation axis $m = l$, or nearby $l = n - 2$, $m = l = n - 2$. Most notably, circular states can have orders of magnitude larger lifetimes than low- l states, ranging into seconds. This has for example been essential in their use for quantum state tomography in cavity quantum electro-dynamics [17–21] and has recently attracted attention in the context of quantum computing [22, 23] or quantum simulations of spin systems [24]. The price paid for the larger lifetime is

a substantially more involved excitation process, which has nonetheless been demonstrated also in an ultracold context [25–28].

Here we determine the utility of a regular assembly of atoms in circular Rydberg states for studies of excitation- and angular momentum transport as well as a platform for flexible Rydberg aggregates. When working in the quasi-hydrogenic manifold of circular states, the many-body electronic Hilbert space can no longer be conveniently simplified based on energetic separation of undesired states. However dipole-dipole selection rules can still allow simple aggregate state spaces consisting of only the two nearest to circular states with $m = n - 1, n - 2$ listed above, where we will study two choices. These both differ from the electronic states considered in [24] (in the $n, n + 2$ manifolds), in that interactions are direct and no two-photon transition is required. We then focus strongly on the implications for exploiting atomic motion.

We theoretically demonstrate clean back and forth transfer of angular momentum within a Rydberg dimer due to the underlying Rabi oscillations between circular states. We also show that in this regime transport can be described both quantum-mechanically and classically, showing good agreement. Interactions between Rydberg atoms in circular states thus might be a further interesting avenue for studies of the quantum-classical correspondence principle with Rydberg atoms [29–34]. Misalignment of the Rydberg aggregate and the electron orbits is shown to cause dephasing of the angular momentum oscillations, that can however be suppressed with small electric fields, as also discussed in [24] for a different choice of states.

We finally explore accessible parameter spaces for Rydberg aggregates based on circular states with the primary focus on flexible Rydberg aggregates (atomic motion), taking into account the main limitations, primar-

*Electronic address: sebastian@iiserb.ac.in

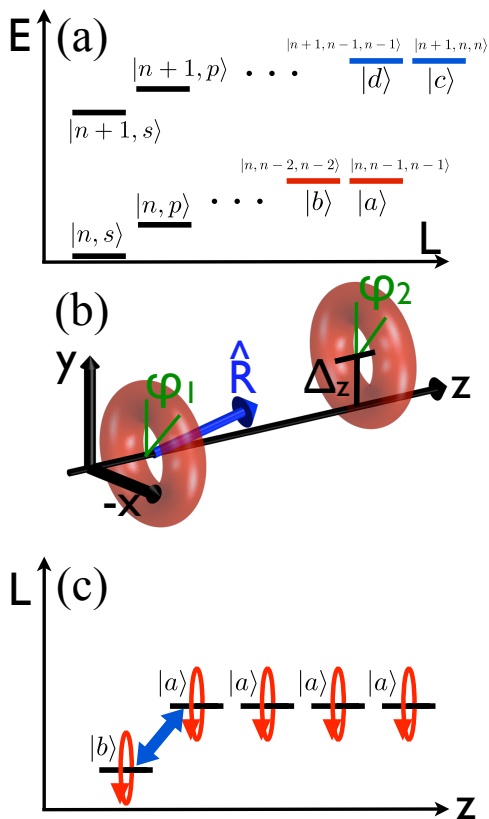


FIG. 1: (a) Schematic energy level diagram of low lying-versus high lying Rydberg states. (b) The shape of the electron probability distribution for circular states with angular momentum pointing fully along the quantisation axis is reminiscent of a circular planetary orbit (red shade). We also indicate various variables discussed in the text. (c) Controlled angular momentum transport on a chain of Rydberg atoms can proceed using only a pair of single atoms states among the high angular momentum manifold.

ily finite lifetime and adjacent n -manifold mixing for too close atomic proximity. We find that flexible aggregates based on circular states offer significantly favorable combinations of lifetime and duration of motional dynamics, despite the weaker interactions, compared to aggregates based on low lying angular momentum states. The number of aggregate atoms could thus be increased to about $N_{\text{agg}} = 100$. To illustrate this we model adiabatic excitation transport on a flexible chain of $N_{\text{agg}} = 20$ atoms.

This article is organized as follows: In section II we introduce circular state atoms and their interactions, leading to a model of excitation transfer on a flexible Rydberg chain. Angular momentum Rabi oscillations in a circular Rydberg dimer are presented in section III, and compared to their classical counterpart. The parameter regimes appropriate for the model in section II A are investigated in section IV, and then demonstrated in section V with an example for angular momentum transport in a large

flexible aggregates.

II. INTERACTIONS OF RYDBERG ATOMS IN CIRCULAR STATES

Consider an electronic Rydberg state with principal quantum number $n \gg 10$ of an Alkali atom, e.g. ^{87}Rb . For a given n , we concentrate on the circular or almost circular states with the two highest allowed values of angular momentum $l = (n-1), (n-2)$. In both cases, angular momentum shall point as much as possible along the quantisation axis, with azimuthal quantum number $m = +l$. In the following, we write triplets of quantum numbers $|n, l, m\rangle$ for electronic states of atoms. Then our states of main interest are $|a\rangle = |n, (n-1), (n-1)\rangle$ and $|b\rangle = |n, (n-2), (n-2)\rangle$. They can be interpreted in terms of Bohr like orbits, with the electron encircling the nucleus on a circular (or very slightly elliptical) orbit, giving rise to the electron probability densities shown in FIG. 1b via their isosurfaces.

Since a spontaneous electric dipole transition can only change the angular momentum by $|\Delta l| = 1$, circular states must decay towards the ground-state through radiative cascades via the nearest angular momentum state and thus exhibit much longer radiative lifetimes τ in vacuum than lower angular momentum (Rydberg) states. This advantage is reduced by black-body radiation at room temperature, which significantly increases the rate for the first transitions of this cascade. Overall we use the formula [22, 35]

$$\tau = \tau_0 / \left(\frac{1}{\exp[\Delta E / (k_B T)] - 1} + 1 \right), \quad (1)$$

where

$$\tau_0 = \frac{24\pi\epsilon_0\hbar^4 c^3}{[E_H^3 a_0^2 e^2]} \frac{(2n-1)^{4n-1}}{2^{4n+1} n^{2n-4} (n-1)^{2n-2}} \quad (2)$$

is the vacuum lifetime, which then gets shortened to the effective lifetime τ by black-body radiation (BBR) at temperature T impacting the first cascade transition of energy gap $\Delta E = E_H/2(1/(n-1)^2 - 1/n^2)$, where E_H is the Hartree energy and a_0 the Bohr radius.

For example the state $|53, 52, 52\rangle$, considered later in this article, has a life time of $\tau = 380 \mu\text{s}$ at $T = 0$ but an effective lifetime $\tau = 2.75 \mu\text{s}$ at $T = 300 \text{ K}$.

While long lifetimes are an attractive feature for quantum simulations involving Rydberg atoms, such simulations rely typically also on a small effective accessible electronic state space per atom, such that each atom can, for example, be considered as a (pseudo) spin-1/2 or spin-1 system. This can be realized by Rydberg $|s\rangle$ ($l=0$) or $|p\rangle$ ($l=1$) states of the same principal quantum number, provided the energy gap to the $|d\rangle$ state is larger than the dynamical energy scales of the problem, which is frequently the case. In contrast, the high angular momentum states become essentially degenerate

approaching Hydrogen states, so simple energetic inaccessibility can no longer be exploited.

However, in principle, interactions can be designed such that still only two circular Rydberg states per atom play a role. This becomes clear by inspection of the dipole-dipole coupling matrix elements, see appendix A and e.g. [36–38]. These couple only two-body states with the same total azimuthal quantum number $M = m_1 + m_2$, as long as the quantisation axis $\hat{\mathbf{z}}$ is oriented along the inter-atomic separation $\hat{\mathbf{R}}$, i.e. when $\hat{\mathbf{z}} \parallel \hat{\mathbf{R}}$. Dipole-dipole interactions (A3) then couple the two pair states $|ab\rangle$, $|ba\rangle$. However, since these are the only pair states with $M = 2n - 3$ for the principal quantum number n manifold, they form a closed subspace.

A. Flexible Rydberg aggregates with circular states

We consider a multi-atom chain as sketched in FIG. 1b,c, where all atoms are as much as possible aligned with the quantisation axis $\hat{\mathbf{z}}$. So the angle θ between the quantisation axis and inter-nuclear axis $\hat{\mathbf{R}}$ is ideally $\theta = 0$, we will, however, consider alignment imperfections $\theta \neq 0$ later. In the ideal case, a single "excitation" in the state $|b\rangle$ can thus migrate through coherent quantum hops through a chain of circular Rydberg atoms in $|a\rangle$. This thus realizes a Rydberg aggregate [1]. Since the number of excitations is conserved, we can describe the aggregate in the basis $|\pi_n\rangle = |aa \cdots b \cdots aa\rangle$, where only the n 'th atom is in the not full circular state $|b\rangle$ and all others in $|a\rangle$.

The effective electronic Hamiltonian can then be written as

$$\hat{H}(\mathbf{R}) = \sum_{n \neq m}^N \frac{C_3^{(ab)}}{|\mathbf{r}_n - \mathbf{r}_m|^3} |\pi_n\rangle \langle \pi_m| + \sum_n E_n(\mathbf{R}) |\pi_n\rangle \langle \pi_n|, \quad (3)$$

$$E_n(\mathbf{R}) = \frac{1}{2} \sum_{j \neq n} \sum_{\ell \neq n, j} \frac{C_6^{(aa)}}{R_{j\ell}^6}, \quad (4)$$

where the first term allows the excitation transport just discussed and the second represents van-der-Waals interactions between atoms in the $|a\rangle$ state.

To describe a flexible aggregate with mobile atoms we solve

$$\hat{H}_{el}(\mathbf{R}) |\varphi_n(\mathbf{R})\rangle = U_n(\mathbf{R}) |\varphi_n(\mathbf{R})\rangle \quad (5)$$

and obtain the excitonic Born-Oppenheimer surfaces $U_n(\mathbf{R})$ that govern the atomic motion, see [1].

It is the main objective of this article to explore the limitations of this simple picture. To this end, we consider the more complete Rydberg-Rydberg interactions that arise from (A3) when taking into account a large range of pair states and imperfect axis alignment. The Hamiltonian \hat{H}_{el} in matrix form (appendix A) is then

diagonalised to give rise to molecular potentials. Some more details are described in appendix A.

For simplicity, we neglect spin-orbit interactions throughout this article. Their presence will not cause large quantitative or qualitative changes from the conclusions reached here.

III. RYDBERG DIMER WITH CIRCULAR STATES

We begin to study angular momentum transport between a pair of Rydberg atoms in circular states for a simple dimer shown in FIG. 1b. We employ the time-dependent Schrödinger equation (TDSE) $i\hbar\partial|\Psi\rangle/\partial t = \hat{H}|\Psi\rangle$, where the Hamiltonian is constructed as discussed in section II and appendix A. Within that space $|\Psi(t)\rangle = \sum_{nlm, n'l'm'} c_{nlm, n'l'm'}(t) |(nlm)_1 (n'l'm')_2\rangle$, where $(nlm)_1$ are quantum numbers of atom 1.

The dimer is initialized in the pair state $|ab\rangle$ for the $n = 53$ manifold. As discussed in section II dipole-dipole interactions can cause a transition to the pair state $|ba\rangle$, giving rise to Rabi-oscillations in an effective two level system, shown in FIG. 2a, if the interatomic axis is perfectly aligned with the quantisation axis ($\theta = 0$). Physically this implies that Rydberg electron orbitals are orthogonal to the interatomic axis. The figure shows the modulus of electronic angular momentum per atom $L_1 = \langle \hat{L}_1 \rangle = \sum_{nlm, n'l'm'} \hbar \sqrt{l(l+1)} |c_{nlm, n'l'm'}|^2$, $L_2 = \langle \hat{L}_2 \rangle = \sum_{nlm, n'l'm'} \hbar \sqrt{l'(l'+1)} |c_{nlm, n'l'm'}|^2$.

The angular momentum exchange can also be modeled classically, using Newton's equation for the Rydberg electrons, with results shown in black. Further details of these simulations can be found in appendix C. Already the simple model employed reproduces the quantum results almost quantitatively. This is expected for circular Rydberg states, since the number of de-Broglie wavelengths fitting into one orbital radius $r_{orb}/\lambda = n$ in Bohr-Sommerfeld theory, which reduces the importance of quantum effects (wave features) for large n , in accordance with the correspondence principle.

The result indicates the utility of interactions among circular Rydberg atoms to illustrate the correspondence principle in action. Once verified in more detail, classical simulations could then supplement quantum ones in the regime where each atom accesses a large number of electronic states, which are challenging quantum mechanically.

In the main part of FIG. 2, we then explore how a misalignment of the circular orbits from the interatomic axis affects angular momentum transport. Since $M = m_1 + m_2$ is no longer conserved in dipole-dipole interactions for that case (see appendix A), a large number of different azimuthal states $m \neq \{n-1, n-2\}$ become populated. This manifests itself in an apparent damping (dephasing) of the oscillations in $L_{1,2}$. We fitted the envelope of oscillations with $\exp[-t^2/\tau_L^2]$ and indicated the resultant τ_L in the figures.

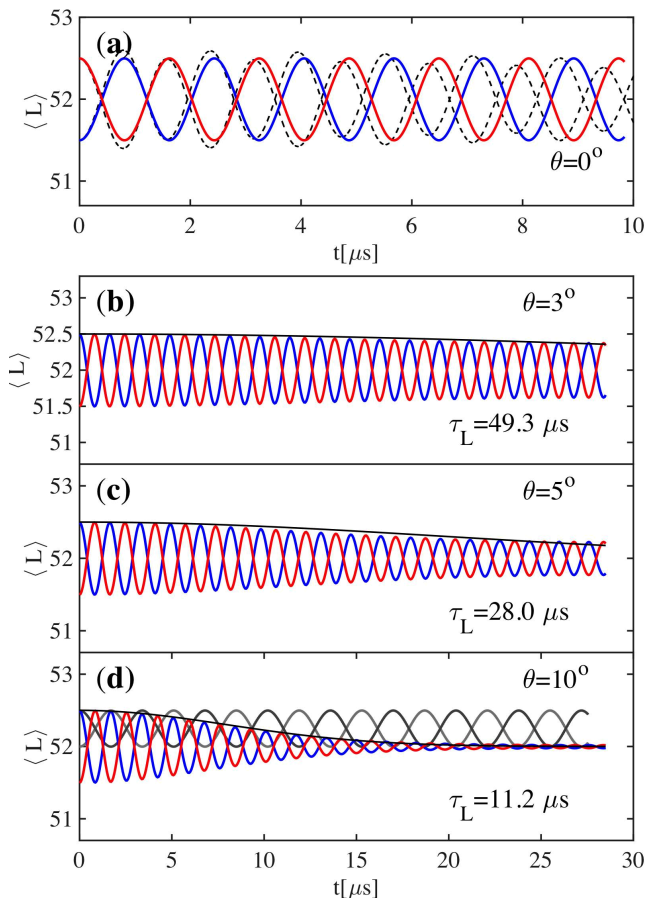


FIG. 2: Angular momentum transport in a dimer of circular state Rydberg atoms separated by $R_0 = 10 \mu\text{m}$. (a) Orbits perfectly aligned with the inter-atomic axis. The angle θ between \hat{R} and \mathbf{z} in FIG. 1b is $\theta = 0^\circ$. Solid lines show the quantum mechanical results for $\langle \hat{L}_1 \rangle$ (blue) and $\langle \hat{L}_2 \rangle$ (red). Black dashed lines are the corresponding angular momenta from the classical Newton's equations, see appendix C. (b) Quantum mechanical angular momenta for a misaligned dimer with $\theta = 3^\circ$. The solid line is a fit on the envelope as discussed in the text. (c) $\theta = 5^\circ$. (d) $\theta = 10^\circ$. The grey lines show the corresponding result in the presence of a small electric field, see text.

Note that even a relative large misalignment such as $\theta = 5^\circ$ still allows many periods of undisrupted angular momentum transport. The coupling to undesired azimuthal state can however be entirely suppressed by the addition of an electric field. This removes the degeneracy of different $|m\rangle$ states through the dc Stark effect [36]. For FIG. 1d we used an electric field amplitude $\mathcal{E} = 0.2 \text{ V/cm}$ and initialised the dimer in $|\Psi(0)\rangle = (|53, 52, 52\rangle|53, 51, 51\rangle + |53, 52, 52\rangle|53, 52, 51\rangle)/\sqrt{2}$. Note that $|\tilde{b}\rangle = (|53, 51, 51\rangle + |53, 52, 51\rangle)/\sqrt{2}$ is the Stark coupled eigenstate corresponding to $|b\rangle$ in the presence of the field. We can see that the Rabi frequency is reduced by a factor of two as expected, since the dipole-dipole interaction couples only the first component of $|\tilde{b}\rangle$ strongly to $|a\rangle$. However in return for this, we retain now

an effective two-level system. Calculations with electric field were streamlined by solving the TDSE only the necessary statespace [39]. Suppressing coupling to undesired m -states through an external field was explored in detail in [24] for coupled states from different (next-to-adjacent) n -manifolds. Here we now extended these concepts to almost circular states from the same n -manifold.

So far, we explored one limitation of the simple picture where only circular states $|ab\rangle$ and $|ba\rangle$ are considered, namely undesired m -levels mixing in through atomic misalignment. This, however, could be circumvented through external electric fields. Another limitation arises at too short distances, where even state manifolds that differ in principal quantum number n are shifted into each other through strong interactions. We show the resultant spectrum in FIG. 3. For demonstration, the figure also shows the detrimental effect on angular momentum transport through this state mixing.

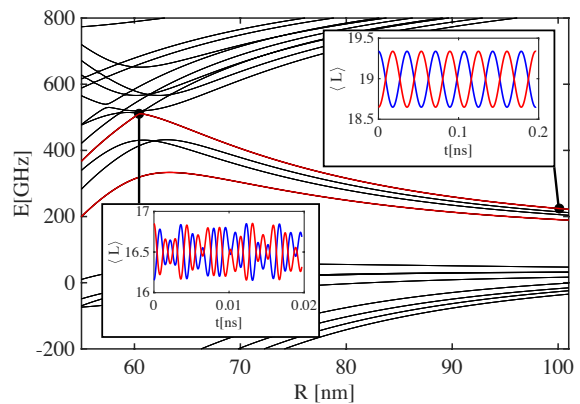


FIG. 3: Interaction potentials of circular Rydberg dimer with $n = 20$ at close proximity. The simple effective state picture involving only two circular states $|a\rangle$ and $|b\rangle$ breaks down once neighboring n manifolds begin to merge into each other around $R = 60 \text{ nm}$. The insets show angular momentum transport akin to FIG. 2a at the indicated separations.

The insets demonstrates how angular momentum oscillations that are regular at distances where adjacent n -manifolds are energetically separate becomes irregular, once all levels begin to mix. We define and calculate the approximate minimal desirable separation d_{min} for atoms in a circular Rydberg aggregate as that distance, where the dipole-dipole shift exceeds the energetic n -manifold separation, see appendix D.

IV. PARAMETER REGIMES FOR CIRCULAR RYDBERG AGGREGATES

We assume now that several Rydberg atoms are aligned in a chain, with all atoms in circular states as shown in FIG. 1c. For conditions explored in the previous section where a single dimer is constrained to the

	$\tilde{C}_3^{(0)}$ [kHz μm^3]	$\tilde{C}_6^{(0)}$ [Hz μm^6]
$ aa\rangle$		2.11×10^{-11}
$ ab\rangle$	2.0	
$ ac\rangle$	0.47	

TABLE I: Interaction parameters for dipole-dipole and van-der-Waals interactions for ^{87}Rb atoms in circular or almost circular Rydberg states.

state-space $|ab\rangle$, $|ba\rangle$, the single $|b\rangle$ state shown in the figure will undergo coherent quantum transport on the chain, without the admixture of any additional many-body states. However we have to now also consider van-der-Waals (vdW) interactions for two atoms in the state $|a\rangle$ (i.e. the energy of $|aa\rangle$). We find these by diagonalising a suitable Hamiltonian as a function of atomic separation R (see appendix A), and then fitting the potential form $E = C_6/R^6$. For dipole-dipole interactions we extract the $|ab\rangle$, $|ac\rangle$ matrix elements from the numerical implementation and verify those also analytically, see appendix B. All these calculations assume an internuclear axis aligned with the quantisation axis $\hat{\mathbf{R}} \parallel \hat{\mathbf{z}}$, which is enough to determine the scale of interactions in a setting such as FIG. 1c.

All interactions exhibit a characteristic scaling with principal quantum number n :

$$C_6 = \tilde{C}_6^{(0)} n^{12}, \quad (6)$$

$$C_3 = \tilde{C}_{3,ab}^{(0)} n^3 \quad \text{for } |ab\rangle, \quad (7)$$

$$C_3 = \tilde{C}_{3,ac}^{(0)} n^4 \quad \text{for } |ac\rangle, \quad (8)$$

which allows their approximate representation in terms of the reference values $\tilde{C}_k^{(0)}$ given in table I. The table distinguishes between dipole-dipole interactions within the same or within adjacent n -manifolds. Note that the scaling of interactions with n is different from that encountered for low-lying angular momentum states, where dipole-dipole interactions always scale as n^4 and van-der-Waals ones as n^{11} [36].

We now follow the approach taken in [1], to delineate different regimes for circular flexible or static Rydberg aggregates based on a variety of requirements that are listed in detail in appendix D. Since dipole-dipole interactions in the pair $|ac\rangle$ substantially exceed those in $|ab\rangle$ for the relevant $n > 20$ due to the steeper scaling in n , we assume an aggregate based on those as in [24]. The results are shown in FIG. 4. It is clear that the use of circular Rydberg atoms for studies involving atomic motion offers substantial advantages. This is, however, the case only in a cryogenic environment at $T \approx 4\text{K}$, since black-body redistribution has a too detrimental effect on the lifetime advantage otherwise. Ideas to suppress spontaneous decay by tuning the electro-magnetic mode structure with a capacitor could improve this situation further [24, 40, 41].

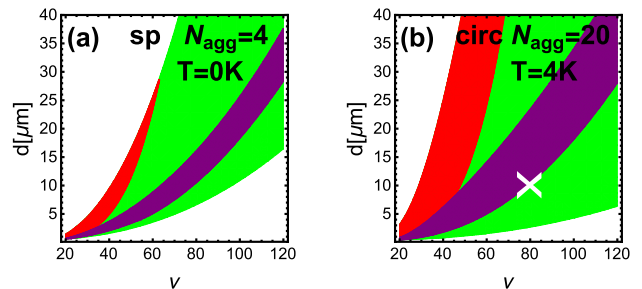


FIG. 4: Parameter domains of static (green and red) versus flexible (violet) Rydberg aggregates. We compare the use of *sp* Rydberg states in (a) versus circular Rydberg states in (b), where the latter are assumed to be in a cryogenic environment (we use $T = 0\text{K}$). Note the substantially different aggregate sizes N_{agg} assumed for either as indicated. Red shade indicates where static aggregates exist, however with atoms that would visibly accelerate during excitation transport. White areas are excluded, either by too short aggregate lifetimes (top) or too close proximities to avoid Rydberg state mixing as in FIG. 3 (bottom). See the text and appendix D for the precise criteria used. The white cross in (b) indicates parameters for FIG. 5.

V. ANGULAR-MOMENTUM TRANSPORT IN LARGE FLEXIBLE RYDBERG AGGREGATES

To illustrate the potential of circular state Rydberg aggregates for studying the coupling between atomic motion and excitation transport, we show a quantum classical simulation of adiabatic excitation transport on a large ($N_{\text{agg}} = 20$) Rydberg aggregate. The parameters are indicated by the white cross in FIG. 4. For similar parameters, even $N_{\text{agg}} = 100$ would still allow end-to-end transport within the lifetime in some parameter range, however, be prohibitive in terms of numerical simulation times.

Adiabatic excitation transport in Rydberg aggregates was thoroughly discussed in [2, 3, 8]. Briefly: a single excited state is initially localized on two atoms at one end of the chain, that are in much closer proximity than all others (here $a = 5\ \mu\text{m}$). The initial repulsion of these atoms causes subsequent repulsive collisions with the remainder of the atoms, the dislocation thus propagating through the chain. The single excitation is carried along with the positional dislocation with high fidelity. This can be traced back to an adiabatic following of the initial dipole-dipole eigenstate $|\varphi_n(\mathbf{R})\rangle$ (see Eq. (5)).

Proposals in [2, 3, 8] were limited by spontaneous decay to about eight Rydberg atoms, even when considering the lighter Li atom. The quantum-classical simulation shown in FIG. 5 highlights that for aggregates from circular states much larger arrays are possible even for the heavier but more common Rb. A detailed description of the algorithm used [42–44] for our purposes can be found in [8, 45].

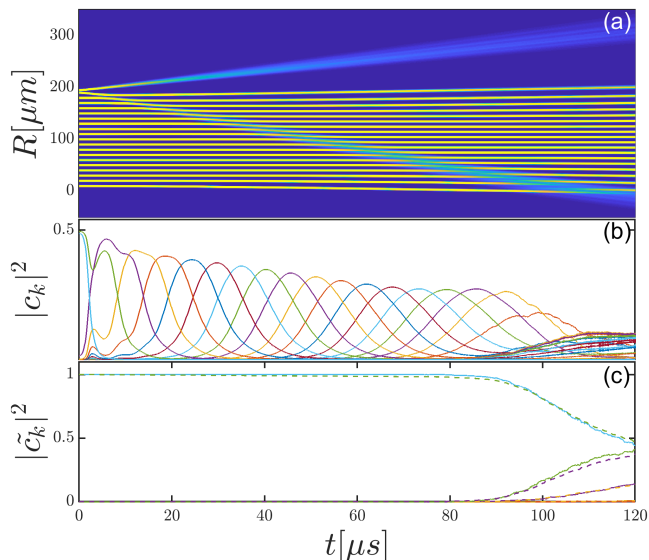


FIG. 5: Adiabatic angular momentum transport on a large flexible Rydberg aggregate with $N = 20$ atoms arranged on a one-dimensional line with spacing $d = 10 \mu\text{m}$, on the repulsive Born-Oppenheimer surface $n = 0$. Each atom has a spatial position uncertainty of $\sigma = \sqrt{\langle \hat{x}^2 \rangle - \langle \hat{x} \rangle^2} = 0.3 \mu\text{m}$. (a) Total density of atoms. (b) Excitation amplitudes on each atom $|c_k|^2 = |\langle \pi_k | \Psi(t) \rangle|^2$. (c) Populations of system eigenstates $|\tilde{c}_k|^2 = |\langle \varphi_n(\mathbf{R}) | \Psi(t) \rangle|^2$ as discussed in section II A, indicating largely adiabatic dynamics.

While the multi-trajectory average in FIG. 5b seems to indicate a loss of fidelity for the excitation transport, this is merely due to the different arrival times for different parts of the many-body wavepacket (different trajectories). We inspected also several individual quantum-classical trajectories, which all show very near 50% population on the two last atoms once the dislocation has fully traversed the chain.

VI. CONCLUSIONS AND OUTLOOK

We assess the utility of arrays of Rydberg atoms in circular and nearly circular angular momentum states for the realisation of flexible Rydberg aggregates. While the motion of circular state Rydberg atoms was considered in [24] as a precursory stage during the creation of regular static arrays, in our work freely moving atoms are the primary focus. There we are interested in studying the inter-relationship between atomic motion and excitation or angular momentum transport. Note that the apparatus proposed in [24] would also be highly suitable for such studies.

In a cryogenic environment (suppressing black-body radiation), circular state flexible Rydberg aggregates will allow much larger arrays of atoms to participate in collective motional dynamics despite their inertia, due to the substantially increased lifetimes. For example, adiabatic excitation transport with high fidelity on chains of

as many as $N_{\text{agg}} = 100$ atoms appears feasible. In the future we will explore the application of this phenomenon for use as a data-bus in circular Rydberg atom based quantum computing architectures [22, 23].

We also demonstrate a case where interacting circular Rydberg atoms can be quite well described using the classical Newton's equations for the Rydberg electrons in a manifestation of the correspondence principle. Both quantum and classical calculations exhibit comparable coherent angular momentum oscillations in a pair of circular Rydberg atoms. More detailed comparisons using more involved classical phase space distributions and quantum wave packets, larger numbers of atoms or more involved geometries could be an interesting exploration of the extent of the correspondence principle. A classical treatment of interactions could then benefit from secular perturbation theory techniques also used in planetary orbital mechanics.

Appendix A: Circular Rydberg interactions

We assume the inter-atomic interactions are entirely based on the dipole-dipole component of the electrostatic Hamiltonian (in atomic units)

$$\hat{H}_{dd} = \frac{\mathbf{r}_1 \cdot \mathbf{r}_2 - 3(\mathbf{r}_1 \cdot \hat{\mathbf{R}})(\mathbf{r}_2 \cdot \hat{\mathbf{R}})}{R^3}, \quad (\text{A1})$$

where $\mathbf{r}_{1,2}$ denote the position of the Rydberg electron in atom 1, 2 and $\hat{\mathbf{R}}$ is a unit vector along the inter-atomic axis, the separation is R , see FIG. 1b. We thus ignore wave-function overlap, core-polarisation or higher order multipoles, as is typical for Rydberg-Rydberg interactions.

We then cast (A2) into a matrix form using pair states $|n_1, l_1, m_1\rangle_1 \otimes |n_2, l_2, m_2\rangle_2$ in a truncated Hilbertspace, where all pair-states are energetically close to those for which we want to determine Rydberg-Rydberg interactions. As usual, the position space representation is written as $\langle \mathbf{r} | n_1, l_1, m_1 \rangle = R_{nl}(r_1) Y_{l_1, m_1}(\theta_1, \varphi_1) / r_1$, where Y are spherical harmonics.

The unperturbed energies of these states are added to the diagonal of the Hamiltonian as $E_{n_1, l_1, m_1} + E_{n_2, l_2, m_2}$ with $E_{n, l, m} = -Ry / (n - \delta_{n, l})^2$, where Ry is the Rydberg constant and $\delta_{n, l}$ the quantum defect taken from [46, 47].

Matrix elements of (A2) are

$$\begin{aligned} & \langle n_1, l_1, m_1; n_2, l_2, m_2 | \hat{H}_{dd} | n'_1, l'_1, m'_1; n'_2, l'_2, m'_2 \rangle \\ &= -8\pi \sqrt{\frac{2\pi}{15}} \frac{d_{n_1, l_1; n'_1, l'_1} d_{n_2, l_2; n'_2, l'_2}}{R^3} \\ & \times \sum_{m_a, m_b} \sum_{\mu=-2}^2 Y_{l=2, \mu}^*(\theta_R, \varphi_R) \langle 1m_1, 1m_2 | 2\mu \rangle \\ & \times \langle l_1, m_1 | Y_{l_1, m_1} | l'_1, m'_1 \rangle \langle l_2, m_2 | Y_{l_2, m_2} | l'_2, m'_2 \rangle, \quad (\text{A2}) \end{aligned}$$

see also [37]. Here θ_R , φ_R are the polar angles of $\hat{\mathbf{R}}$ in the 3D spherical coordinate system defining n, l, m , $\langle 1m_1, 1m_2 | 2\mu \rangle$ the Clebsch-Gordan coefficient coupling two constituent angular momenta ($l = 1, m = m_{1,2}$) to a total angular momentum ($L = 2, M = \mu$) and the integrals in the last line involve now a single electronic co-ordinate and three spherical harmonics each.

Evaluating these as in [48], we use

$$\begin{aligned} \langle l_1, m_1 | Y_{1m_1} | l'_1, m'_1 \rangle &= (-1)^m \sqrt{\frac{3(2l_1 + 1)(2l'_1 + 1)}{4\pi}} \\ &\times \begin{pmatrix} l_1 & l'_1 & 1 \\ 0 & 0 & 0 \end{pmatrix} \begin{pmatrix} l'_1 & l_1 & 1 \\ m'_1 & -m_1 & m_1 \end{pmatrix}, \quad (\text{A3}) \end{aligned}$$

where terms in brackets denote Wigner $3j$ symbols.

The $d_{n_1, l_1; n'_1, l'_1} = \int_0^\infty r R_{n_1, l_1}(r) R_{n'_1, l'_1}(r) dr$ in (A2) are radial matrix elements, determined via the Numerov method including modifications of the Coulomb potential due to the core as in [46]. To avoid instabilities, the solutions R are set to zero inside the inner classical turning point for large l .

When considering interactions within an external electric fields, we describe the field through single body matrix elements

$$\begin{aligned} -\langle n, l, m | \mathcal{E} \hat{z} | n', l', m' \rangle &= -d_{n, l; n', l'} \sqrt{\frac{3(2l + 1)(2l' + 1)}{4\pi}} \\ &\times \begin{pmatrix} l & l' & 1 \\ 0 & 0 & 0 \end{pmatrix} \begin{pmatrix} l' & l & 1 \\ m' & -m & 0 \end{pmatrix}, \quad (\text{A4}) \end{aligned}$$

To obtain vdW interaction potentials, the resultant dimer Hamiltonian is diagonalized as a function of separation R , see e.g. FIG. 3. For transport simulations, the restricted basis Hamiltonian is constructed at a fixed separation R_0 and then used in the time-dependent Schrödinger equation.

A recent numerical package for these sort of calculations is described in [49]. For low lying state interaction, also perturbation theory can be used [50].

Appendix B: Calculation of dipole-dipole interaction constants

For circular states of Alkali atoms, the wave function overlap with the core becomes so small that the use of Hydrogen wave functions $\Psi(r_k, \theta_k, \varphi_k) = R_{nl} Y_{lm}(\theta, \varphi) / r_k$, where $k \in \{1, 2\}$ numbers the atom, becomes highly justified. We can then determine e.g. $C_{3, ab}$ coefficients from Eq. (A2) by inserting the appropriate sets of quantum numbers for $\langle ab | \hat{H}_{dd} | ba \rangle$.

Since $\hat{\mathbf{R}} \parallel \hat{\mathbf{z}}$ we have $\theta = 0$. In that case, only the pre-factor of $Y_{l=2,0}^*(\theta = 0, \varphi)$ with $\mu = 0$ fulfills all angular momentum selection rules in (A2), yielding the integral

$$I = \langle 1, 1; 1, -1 | 2, 0 \rangle \langle a | Y_{1,1} | b \rangle \langle b | Y_{1,-1} | a \rangle, \quad (\text{B1})$$

which results in

$$\begin{aligned} I &= \frac{(-1)^{2(2n-3)} (2n-1)(2n-3)(2n-2)!(2n-4)!}{2^{2(2n-3)} ((n-1)!(n-2)!)^2} \\ &\times \left(\frac{1}{4\pi}\right)^2 \left(-\frac{3(2\pi)^2}{8\pi\sqrt{6}}\right) \left(\frac{\sqrt{\pi}\Gamma(n)}{\Gamma(n+\frac{1}{2})}\right)^2, \quad (\text{B2}) \end{aligned}$$

where $\Gamma(n)$ is the Gamma function. Using $Y_{2,0}^*(\theta = 0, \varphi) = \sqrt{\frac{5}{4\pi}}$ and the radial matrix element

$$\begin{aligned} d_{n_a l_a, n_b l_b} &= \int_0^\infty r (r R_{n_a, l_a}(r)) (r R_{n_b, l_b}(r)) dr \\ &= -\frac{3n}{2} \sqrt{(2n-1)}, \quad (\text{B3}) \end{aligned}$$

we finally reach

$$\begin{aligned} V_{ab;ba} &= -\frac{8\pi}{R^3} \sqrt{\frac{2\pi}{15}} \sqrt{\frac{5}{4\pi}} \left(\frac{-3n}{2} \sqrt{(2n-1)}\right)^2 \\ &\times \frac{(-1)^{2(2n-3)} (2n-1)(2n-3)(2n-2)!(2n-4)!}{2^{2(2n-3)} ((n-1)!(n-2)!)^2} \\ &\times \left(\frac{1}{4\pi}\right)^2 \left(-\frac{3(2\pi)^2}{8\pi\sqrt{6}}\right) \left(\frac{\sqrt{\pi}\Gamma(n)}{\Gamma(n+\frac{1}{2})}\right)^2, \quad (\text{B4}) \end{aligned}$$

which agrees with the results from the numerical implementation of (A2) discussed in section A.

See [22] for analytical results for the $|aa\rangle \leftrightarrow |cc'\rangle$ dipole-matrix elements, where $|c'\rangle = |n-1, n-2, n-2\rangle$.

Appendix C: Classical Simulations of Rydberg Dimer

In the classical simulations, we adopted the Bohr-Sommerfeld atomic model to mimic the orbital behaviour by using elliptical orbits for a classical point electron. Initial positions and velocities are drawn from a random distribution that respects the target quantum numbers via energy and (angular momentum):

$$E_n = -\frac{e^4 m_e}{32\pi^2 \epsilon_0^2 \hbar^2 n^2}, \quad (\text{C1})$$

$$L_m = \hbar \sqrt{l(l+1)}, \quad (\text{C2})$$

where m_e is the mass of the electron.

In the model, the electron follows an elliptic path and the semi-major (a) and semi-minor (b) axes are defined as:

$$a_n = \frac{4\pi\epsilon_0 \hbar^2}{m_e e^2} n^2, \quad b_{nl} = \frac{l}{n} a_n. \quad (\text{C3})$$

In the simulation, nuclei of the atoms are assumed to be motionless and the equation of motion for the electrons is

$$\ddot{\mathbf{r}}_{ei} = -\frac{e^2}{4\pi\epsilon_0 m_e} \left(\frac{\mathbf{r}_{ei} - \mathbf{r}_{ni}}{\|\mathbf{r}_{ei} - \mathbf{r}_{ni}\|^3} + \frac{\mathbf{r}_{ei} - \mathbf{r}_{n(i+1)}}{\|\mathbf{r}_{ei} - \mathbf{r}_{n(i+1)}\|^3} - \frac{\mathbf{r}_{ei} - \mathbf{r}_{e(i+1)}}{\|\mathbf{r}_{ei} - \mathbf{r}_{e(i+1)}\|^3} \right), \quad (\text{C4})$$

where the index ni is the i^{th} nucleus and the index ei is the i^{th} electron. The notation $(i+1)$ pertains here simply to the adjacent atom in a dimer.

The classical simulation is conducted by numerical evaluation of the equation of motion and averaging the results over random initial positions of the electron on the elliptic orbit. For this we vary in particular the relative orbital phase between the electrons, $\varphi_2 - \varphi_1$, see FIG. 1b.

The black dashed lines in FIG. 2a show finally the ensemble averaged angular momenta $L_k = |\overline{\mathbf{L}_k}|$, where \mathbf{L}_k is the angular momentum of electron k with respect to nucleus k . The model could be made more sophisticated by incorporating also the out of plane distribution of the Rydberg electron evident in FIG. 1b or nuclear motion.

Appendix D: Parameter constraints for Rydberg aggregates

For the parameter space surveys in section IV we have utilised the following mathematical criteria to define when a one-dimensional circular Rydberg atom chain can constitute a useful flexible Rydberg aggregate. We

are following the approach of [1]. *Validity of the essential state model:* We have seen in FIG. 3 that the essential state model based on $|a\rangle$, $|b\rangle$ breaks down once adjacent n -manifolds begin to mix. We have taken the corresponding distance d_{min} as the one where $C_3(n)/d_{\text{min}}^3 = 1/(2\nu^2) - 1/(2(\nu+1)^2)$ (atomic units).

Static aggregates: From (7) we can infer a transfer time (Rabi oscillation period) $T_{\text{hop}} = \pi d^3/C_3$ for an excitation to migrate from a given atom to the neighboring one, if the inter-atomic spacing is d . We have calculated the corresponding time for $N_{\text{hops}} = 100$ such transfers, given by $T_{\text{trans}} = N_{\text{hops}} T_{\text{hop}}$, imagining migration along an entire aggregate. We finally require T_{trans} to be short compared to the system lifetime, which is determined for circular states based on Eq. (1).

Perturbing acceleration: The characteristic time for atom acceleration is $T_{\text{acc}} = \sqrt{\frac{R_0^5 M}{6C_3}}$ [1], with mass of the atoms M and their initial separation R_0 . We then color the parameter space red in FIG. 4, where atoms would inadvertently be set into motion due to $4T_{\text{acc}} < T_{\text{trans}}$.

Flexible aggregates: For flexible aggregates, we assume an equidistant chain with spacing d , but the existence of a dislocation on the first two atoms with spacing of only $d_{\text{ini}} = 2d/3$ to initiate directed motion, similar to section V. Hence, $d_{\text{ini}} > d_{\text{min}}$ must be fulfilled, a tighter constraint than $d > d_{\text{min}}$. We can then assess as in [1] whether an excitation transporting pulse can traverse the chain within the system lifetime.

Acknowledgments

We gratefully acknowledge fruitful discussions with Mehmet Oktel and Michel Brune.

-
- [1] S. Wüster and J. M. Rost, J. Phys. B **51**, 032001 (2018).
 - [2] S. Wüster, C. Ates, A. Eisfeld, and J. M. Rost, Phys. Rev. Lett. **105**, 053004 (2010).
 - [3] S. Möbius, S. Wüster, C. Ates, A. Eisfeld, and J. M. Rost, J. Phys. B **44**, 184011 (2011).
 - [4] S. Wüster, Phys. Rev. Lett. **119**, 013001 (2017).
 - [5] D. W. Schönleber, A. Eisfeld, M. Genkin, S. Whitlock, and S. Wüster, Phys. Rev. Lett. **114**, 123005 (2015).
 - [6] S. Wüster, A. Eisfeld, and J. M. Rost, Phys. Rev. Lett. **106**, 153002 (2011).
 - [7] K. Leonhardt, S. Wüster, and J. M. Rost, Phys. Rev. Lett. **113**, 223001 (2014).
 - [8] K. Leonhardt, S. Wüster, and J. M. Rost, Phys. Rev. A **93**, 022708 (2016).
 - [9] K. Leonhardt, S. Wüster, and J. M. Rost, J. Phys. B **50**, 054001 (2017).
 - [10] H. Zoubi, A. Eisfeld, and S. Wüster, Phys. Rev. A **89**, 053426 (2014).
 - [11] D. Barredo, H. Labuhn, S. Ravets, T. Lahaye, A. Browaeys, and C. S. Adams, Phys. Rev. Lett. **114**, 113002 (2015).
 - [12] H. Labuhn, D. Barredo, S. Ravets, S. de Léséleuc, T. Macrì, T. Lahaye, and A. Browaeys, Nature **534**, 667 (2016).
 - [13] S. Bettelli, D. Maxwell, T. Fernholz, C. S. Adams, I. Lesanovsky, and C. Ates, Phys. Rev. A **88**, 043436 (2013).
 - [14] D. Maxwell, D. J. Szwer, D. Paredes-Barato, H. Busche, J. D. Pritchard, A. Gauguet, K. J. Weatherill, M. P. A. Jones, and C. S. Adams, Phys. Rev. Lett. **110**, 103001 (2013).
 - [15] G. Günter, H. Schempp, M. Robert-de-Saint-Vincent, V. Gavryusev, S. Helmrich, C. S. Hofmann, S. Whitlock, and M. Weidemüller, Science **342**, 954 (2013).
 - [16] A. P. Orioli, A. Signoles, H. Wildhagen, G. Günter, J. Berges, S. Whitlock, and M. Weidemüller, Phys. Rev. Lett. **120**, 063601 (2018).
 - [17] M. Brune, S. Haroche, V. Lefevre, J. M. Raimond, and N. Zagury, Phys. Rev. Lett. **65**, 976 (1990).
 - [18] M. Brune, J. Bernu, C. Guerlin, S. Deléglise, C. Sayrin,

- S. Gleyzes, S. Kuhr, I. Dotsenko, J. M. Raimond, and S. Haroche, *Phys. Rev. Lett.* **101**, 240402 (2008).
- [19] M. Brune, S. Haroche, J. M. Raimond, L. Davidovich, and N. Zagury, *Phys. Rev. A* **45**, 5193 (1992).
- [20] S. Gleyzes, S. Kuhr, C. Guerlin, J. Bernu, S. Deléglise, U. B. Hoff, M. Brune, J.-M. Raimond, and S. Haroche, *Nature* **446**, 297 (2007).
- [21] S. Deléglise, I. Dotsenko, C. Sayrin, J. Bernu, J.-M. Raimond, and S. Haroche, *Nature* **455**, 510 (2008).
- [22] T. Xia, X. L. Zhang, and M. Saffman, *Phys. Rev. A* **88**, 062337 (2013).
- [23] M. Saffman, *Journal of Physics B: Atomic, Molecular and Optical Physics* **49**, 202001 (2016).
- [24] T. L. Nguyen, J. M. Raimond, C. Sayrin, R. Cortiñas, T. Cantat-Moltrecht, F. Assemat, I. Dotsenko, S. Gleyzes, S. Haroche, G. Roux, et al., *Phys. Rev. X* **8**, 011032 (2018).
- [25] D. A. Anderson, A. Schwarzkopf, R. E. Sapiro, and G. Raithel, *Phys. Rev. A* **88**, 031401(R) (2013).
- [26] P. Nussenzveig, F. Bernardot, M. Brune, J. Hare, J. Raimond, S. Haroche, and W. Gawlik, *Physical Review A* **48**, 3991 (1993).
- [27] R. Brecha, G. Raithel, C. Wagner, and H. Walther, *Optics Communications* **102**, 257 (1993).
- [28] V. Zhelyazkova and S. Hogan, *Physical Review A* **94**, 023415 (2016).
- [29] Z. D. Gaeta and C. R. Stroud, *Phys. Rev. A* **42**, 6308 (1990).
- [30] T. P. Hezel, C. E. Burkhardt, M. Ciocca, L. He, and J. J. Leventhal, *American Journal of Physics* **60**, 329 (1992).
- [31] T. P. Hezel, C. E. Burkhardt, M. Ciocca, and J. J. Leventhal, *American Journal of Physics* **60**, 324 (1992).
- [32] I. Samengo, *Phys. Rev. A* **58**, 2767 (1998).
- [33] M. Bucher (2008), <https://arxiv.org/abs/0802.1366>.
- [34] T. Deeney and C. O'Sullivan, *American Journal of Physics* **82**, 883 (2014).
- [35] I. I. Beterov, I. I. Ryabtsev, D. B. Tretyakov, and V. M. Entin, *Phys. Rev. A* **79**, 052504 (2009).
- [36] T. F. Gallagher, *Rydberg Atoms* (Cambridge University Press, 1994).
- [37] F. Robicheaux, J. V. Hernandez, T. Topcu, and L. D. Noordam, *Phys. Rev. A* **70**, 042703 (2004).
- [38] N. Šibalić, J. D. Pritchard, C. S. Adams, and K. J. Weatherill, *Comp. Phys. Comm.* **220**, 319 (2017).
- [39] We collect all states that are coupled to the initial state via just $c = 3$ coupling matrix elements. Of these we also remove all that are detuned by more than $E_{\text{cut}} = 2000$ Mhz. Finally we verified that results do not change when these numerical constraints were loosened.
- [40] D. Kleppner, *Phys. Rev. Lett.* **47**, 233 (1981).
- [41] R. G. Hulet, E. S. Hilfer, and D. Kleppner, *Phys. Rev. Lett.* **55**, 2137 (1985).
- [42] J. C. Tully, *The Journal of Chemical Physics* **93**, 1061 (1990).
- [43] J. C. Tully and R. K. Preston, *The Journal of Chemical Physics* **55**, 562 (1971).
- [44] M. Barbatti, *Wiley Interdisciplinary Reviews: Computational Molecular Science* **1**, 620 (2011).
- [45] K. Leonhardt (2016), thesis online at <https://arxiv.org/abs/1612.07858>.
- [46] T. Amthor (2008), thesis online at <https://freidok.uni-freiburg.de/data/5802>.
- [47] W. Li, I. Mourachko, M. W. Noel, and T. F. Gallagher, *Phys. Rev. A* **67**, 052502 (2003).
- [48] I. S. Gradshteym and I. M. Ryzhik, *Table of Integrals, Series and Products* (Academic Press, London, UK, 2007).
- [49] S. Weber, C. Tresp, H. Menke, A. Urvoy, O. Firstenberg, H. P. Büchler, and S. Hofferberth, *J. Phys. B* **50**, 133001 (2017).
- [50] K. Singer, J. Stanojevic, M. Weidemüller, and R. Côté, *J. Phys. B* **38**, S295 (2005).